Sciencexpress Reports

High-performance photovoltaic perovskite layers fabricated through intramolecular exchange

Woon Seok Yang,[1]* Jun Hong Noh,[1]* Nam Joong Jeon,[1] Young Chan Kim,[1] Seungchan Ryu,[1] Jangwon Seo,[1] Sang Il Seok[1,2]†

[1]Division of Advanced Materials, Korea Research Institute of Chemical Technology, 141 Gajeong-Ro, Yuseong-Gu, Daejeon 305-600, Korea. [2]Department of Energy Science, Sungkyunkwan University, Suwon 440-746, Republic of Korea.

†Corresponding author. E-mail: seoksi@krict.re.kr (seoksi@skku.edu)

*These authors contributed equally to this work.

The band gap of formamidinium lead iodide ($FAPbI_3$) perovskites allows broader absorption of the solar spectrum compared to conventional methylammonium lead iodide ($MAPbI_3$). The optoelectronic properties of perovskite films are closely related to the film-quality, so depositing dense and uniform films is crucial for fabricating high-performance perovskite solar cells (PSCs). We report an approach for depositing high-quality $FAPbI_3$ films, involving $FAPbI_3$ crystallization by the direct intramolecular exchange of dimethylsulfoxide (DMSO) molecules intercalated in PbI_2 with formamidinium iodide. This process produces $FAPbI_3$ films with (111)-preferred crystallographic orientation, large-grained dense microstructures, and flat surfaces without residual PbI_2. Using films prepared by this technique, $FAPbI_3$-based PSCs with maximum power conversion efficiency of over 20% were fabricated.

The tremendous improvements in device architecture (*1*–*3*), high-quality film formation methodologies (*4*–*6*), and compositional engineering of perovskite materials (*7*–*9*) over the last 3 years have led to rapid improvements in the power conversion efficiency (PCE) of perovskite solar cells (PSCs). Although solar-to-electric PCE of up to 18% has been reported for PSCs (*10*), developing technologies further to achieve PCEs near theoretical values continues to be among the most important challenges in the solar cell industry to achieve economic feasibility.

Formamidinium lead iodide ($FAPbI_3$) is a perovskite material that can potentially provide better performance than methylammonium lead iodide ($MAPbI_3$) because of its broad absorption of the solar spectrum. In addition, $FAPbI_3$ with the n-i-p architecture (the n-side is illuminated with solar radiation) exhibits negligible hysteresis with sweep direction during current-voltage measurements (*8*–*13*). However, compared to $MAPbI_3$, it is more difficult to form stable perovskite phases and high-quality films of $FAPbI_3$. Various methodologies such as sequential deposition (*4*), solvent-engineering (*5*), vapor-assisted deposition (*14*), additive-assisted deposition (*15*, *16*), and vacuum evaporation (*6*) can now produce high-quality films of $MAPbI_3$ with flat surfaces and complete surface coverage by controlling its rapid crystallization behavior and have led to substantial improvements in the PCE of $MAPbI_3$-based PSCs.

Among these methodologies, two-step sequential deposition and solvent-engineering are representative wet processes that can yield perovskite films for high-performance PSCs. In the sequential deposition process, a thin layer of PbI_2 is deposited on the substrate. methylammonium iodide (MAI) or formamidinium iodide (FAI) is then applied to the pre-deposited PbI_2 to enable conversion to the perovskite phase. This process involves crystal nucleation and growth of the perovskite phase because of solution-phase or solid-state reaction between PbI_2 and an organic iodide such as MAI or FAI (*4*, *13*, *17*). However, the sequential reaction of organic iodides with PbI_2 that occurs from the surface to the inner crystalline regions of PbI_2 has been ineffective in producing high-performance perovskite films that are > 500 nm in thickness because of incomplete conversion of PbI_2, peeling-off of the perovskite film in solution, and uncontrolled surface roughness. In contrast, the solvent-engineering process utilizes the formation of intermediate phases to retard the rapid reaction between PbI_2 and organic iodide in the solution. While this process has been successfully used to form dense and uniform $MAPbI_3$ layers, it has not been explored for $FAPbI_3$ (*5*).

To deposit a uniform and dense $FAPbI_3$ layer, Snaith *et al.* added a small amount of aqueous HI to a solution mixture containing PbI_2, FAI, and dimethylformamide (DMF) (*11*). Very recently, Zhao *et al.* reported the deposition of highly uniform and fully covered $FAPbI_3$ films using FAI and $HPbI_3$, which is formed by the reaction of PbI_2 and HI in DMF (*18*). The HI in the PbI_2 layers retards the rapid reaction between FAI and PbI_2. In addition, the release of HI from PbI_2 at high temperatures allows the formation of a $FAPbI_3$ layer by solid-state reaction with the neighboring FAI molecules. Stated differently, this process can be regarded as the transformation of PbI_2-HI-FAI into $FAPbI_3$, similar to the formation of $MAPbI_3$ via the PbI_2-dimethylsulfoxide (DMSO)-MAI phase in the solvent-engineering process (*5*).

However, we observed that the solvent-engineering process, which is effective for depositing dense and uniform $MAPbI_3$ layers, yields $FAPbI_3$ layers with pin-holes and a

rough surface. Although the $FAPbI_3$ film-quality including coverage and uniformity on the substrate have been improved, the performance of $FAPbI_3$-solar cells still lag behind those of $MAPbI_3$-based PSC (*8*), implying that more sophisticated deposition techniques are necessary for fabricating high-quality, thick $FAPbI_3$ films (> 500 nm), for achieving sufficient absorption up to a wavelength of 840 nm.

As expected from the conversion of PbI_2-DMSO-MAI to $MAPbI_3$ (*5*), the DMSO molecules intercalated in PbI_2 can be easily replaced by external FAIs because of its higher affinity toward PbI_2 compared to DMSO; the FAI molecules experience ionic interactions, whereas DMSO participates in van der Waals interactions (*5*, *19*). Highly uniform and dense pre-deposited PbI_2-(DMSO) layers could be directly converted to $FAPbI_3$ because the inorganic PbI_2 framework would be retained. $FAPbI_3$ crystallization by the intramolecular exchange process (IEP) of DMSO intercalated in PbI_2 with FAI was schematically shown in Fig. 1A. The intramolecular exchange between DMSO and FAI can be described as

$$PbI_2{-}DMSO + FAI \rightarrow PbI_2{-}FAI + DMSO \uparrow (\text{removal}) \quad (1)$$

and does not induce volume expansion, unlike the $FAPbI_3$ formed with FAI intercalating into pristine PbI_2 (discussed below) because the molecular sizes of DMSO and FAI are similar.

In this work, we report on the synthesis of a PbI_2-(DMSO) precursor with excellent capabilities for molecular exchange with FAI at low temperatures during the spinning process, as well as the fabrication of highly efficient $FAPbI_3$-based PSCs with certified PCEs exceeding 20%. To synthesize the PbI_2-(DMSO) precursors, precipitates were obtained by pouring toluene as a non-solvent into 1.0 M PbI_2 solution dissolved in DMSO. The x-ray diffraction (XRD) pattern of the resulting complex (Fig. 1Ba) matched that of the $PbI_2(DMSO)_2$ phase (*5*, *19*). The as-prepared $PbI_2(DMSO)_2$ was then annealed at 60°C for 24 hours in vacuum to obtain PbI_2(DMSO) by removal of 1 mol DMSO. The XRD pattern of the vacuum-annealed powder (Fig. 1Bb) did not match that of $PbI_2(DMSO)_2$, implying that the $PbI_2(DMSO)_2$ transformed into a different phase by releasing some DMSO molecules. The content of DMSO in the as-annealed powder was estimated by thermogravimetric analysis (TGA). TGA was suitable for this purpose because the only volatile species in the powder was DMSO. The TGA results of the $PbI_2(DMSO)_2$ and PbI_2(DMSO) complexes are shown in Fig. 1C. The $PbI_2(DMSO)_2$ complex exhibited a two-step decomposition process with weight-loss of 12.6% at each step, whereas the vacuum-annealed PbI_2(DMSO) complex showed a single-step decomposition. The decomposition of both the complexes was completed at the same temperature (138. 6°C). The powders obtained by vacuum-annealing $PbI_2(DMSO)_2$ complex at 60°C can be regarded as one of the most thermodynamically stable forms among the various crystalline PbI_2-(DMSO)-based complexes, which are similar with $PbBr_2$(DMSO) and $PbCl_2$(DMSO) (*20*). The DMSO content of the vacuum-annealed PbI_2(DMSO) complex was also checked by elemental analysis (EA), which yielded H = 1.0% (1.1%); and C = 4.1% (4.4%), where the values expressed in parenthesis indicate the theoretical mass percent for a given element for $C_2H_6SOPbI_2$.

To fabricate $FAPbI_3$-based PSCs through IEP between DMSO and FAI (MABr) using pre-deposited PbI_2-DMSO layers and a FAI (MABr) solution, we first confirmed that the PbI_2(DMSO) phase was retained even after spin-coating with the PbI_2(DMSO) precursor dissolved in DMF. The XRD pattern for film coated on a fused silica substrate was compared with that of the initial precursor. As seen in Fig. 1Bc, the XRD pattern for the as-coated film was in consistent with that of the PbI_2(DMSO) complex powder, although its crystallinity is lowered. The as-coated PbI_2(DMSO) film also had a flat and dense surface, as shown in the field-emission scanning electron microscopy (FESEM) image in fig. S1 (*21*). Next, we investigated the formation of mixed $FAPbI_3/MAPbBr_3$ by IEP. We recently reported that the coexistence of MA/FA/I/Br in the PbI_2 skeleton improved the phase-stability of $FAPbI_3$ (*10*). The formation of mixed $FAPbI_3/MAPbBr_3$ layers via IEP was controlled by coating solution mixture with different mole ratios of MABr to FAI dissolved in isopropyl alcohol (IPA), on the pre-deposited PbI_2(DMSO) layers (discussed below). It is evident from Fig. 1Da that well-crystallized $FAPbI_3$-based films were formed by IEP. The XRD pattern for the $FAPbI_3$ film derived from the PbI_2(DMSO) complex film exhibits dominant (-111) and (-222) diffraction peaks at 13.9° and 28.1°, respectively, corresponding to the $FAPbI_3$ trigonal perovskite phase (P3m1), in contrast with the XRD patterns of the $FAPbI_3$ powder (Fig. 1Db) (*13*). The intensity ratio of (-123) peak at 31.5 ° to the (-222) peak at 28.1° was 0.05. This value was much smaller than the corresponding intensity ratios (= 0.8) for the $FAPbI_3$ power. Thus, IEP leads to high-quality pure $FAPbI_3$–based films with preferred orientation along the [111] axis.

Fig. S2 (*21*) presents the current density–voltage (*J–V*) curves measured under standard air-mass 1.5 global (AM 1.5G) illumination, and the external quantum efficiency (EQE) spectra of the fabricated cells with $FAPbI_3$–based layers fabricated with various amounts of MABr (0 to 20 mol%). The onset wavelength in the EQE spectra near 830 nm showed a non-linear blue shift with increasing amounts of MABr, indicating that there is unsymmetrical competition between FAI and MABr in forming the $FAPbI_3$-$MAPbBr_3$ perovskite phase through an intramolecular exchange reaction. Nevertheless, the highest PCE of 19.2% was achieved for the film fabricated from a FAI solution containing 15 mol% MABr. To accurately determine the composition of the $FAPbI_3$–based layer, we investigated the lattice parameter using XRD and the band gap using the EQE for the film showing the best performance. Fig. S3 (*21*) shows the pseudocubic lattice parameter for $(FAPbI_3)_{1-x}(MAPbBr_3)_x$ as a function of *x*, in which the composition was controlled

by a previously reported method (*10*). In this study, the pseudocubic lattice parameter of the $FAPbI_3$/$MAPbBr_3$ film fabricated by IEP with a FAI solution containing 15 mol% MABr is 6.348 Å. As indicated in fig. S4 (*21*), the lattice parameter can be assigned as x = ~ 5, corresponding to $(FAPbI_3)_{0.95}(MAPbBr_3)_{0.05}$. This result is in agreement with the value estimated using the band gap (1.49 eV) from EQE [fig. S3 (*21*)], because pure $FAPbI_3$ has a band gap of 1.47 eV and $(FAPbI_3)_{0.85}(MAPbBr_3)_{0.15}$, 1.55 eV (*10*). Fortunately, the simultaneous introduction of both MA^+ cations and Br^- anions in $FAPbI_3$ even after incorporating 5 mol% of $MAPbBr_3$ serves to stabilize the perovskite phase (*10*).

After comparing the absorption coefficients of $FAPbI_3$ and $MAPbI_3$ at wavelengths beyond 800 nm, we noted that the thickness of a $FAPbI_3$ layer needed to be higher than the optimal thickness of a typical perovskite layer with a band gap of ~1.55 eV (300 to 400 nm) to guarantee fully light-harvesting around 800 nm (*20*, *22*). We deposited $FAPbI_3$–based layers with thickness of ~ 500 nm, and fabricated devices consisting of fluorine-doped tin oxide (FTO)-glass/barrier layer (bl)-TiO_2/mesoporous (mp)-TiO_2/perovskite/poly-triarylamine (PTAA)/Au (n-i-p architecture), as shown in the cross-sectional FESEM image of Fig. 2A. FESEM plane-view images of the device with film derived from PbI_2(DMSO) complex and PbI_2 films are shown in Fig. 2B. The $FAPbI_3$ film derived from PbI_2(DMSO) exhibited a dense and well-developed grain structure with larger grains than the $FAPbI_3$ film derived from PbI_2. Figure 2Ca shows the *J-V* curves measured via reverse and forward bias sweep for one of the best-performing solar cell. The devices we fabricated also showed no hysteresis. Here, we believe that the hysteresis is highly dependent on the perovskite materials ($FAPbI_3$ or $MAPbI_3$) and cell architecture (n-i-p or p-i-n), although the ferroelectric properties of the perovskite itself are more likely to be the origin of the hysteresis in PSCs (*23*, *24*). Thus, $FAPbI_3$-based PSCs with n-i-p architecture show negligible hysteresis between the reverse and the forward scan in the I-V characteristics. In contrast, $FAPbI_3$-based cells consisting of FTO/NIO/ perovskite/PCBM/LiF/Al (p-i-n architecture) showed very strong hysteresis [fig. S4 (*21*)]. J_{SC}, V_{OC}, and *FF* determined from the *J-V* curves were 24.7 mA cm^{-2}, 1.06 V, and 77.5%, respectively, and correspond to a PCE of 20.2% under standard AM 1.5G illumination. Figure 2Cb shows the EQE spectrum and integrated J_{SC} for one of the best-performing solar cell. The high J_{SC} is attributed to a very broad EQE plateau of >85% in the illumination wavelength range of 400 to 780 nm and broad light-harvesting up to a long wavelength of 840 nm, owing to the relatively low band gap (1.47 eV) of $FAPbI_3$. The J_{SC} value (24.4 mA cm^{-2}) obtained by integrating EQE spectrum agreed well with that derived from the *J-V* measurement. The PCE of the best-performing cell (20.2%) was certified by the standardized method in the PV calibration laboratory, which confirmed a PCE of 20.1% under AM 1.5 G full-sun illuminations [fig. S5 (*21*)].

To gain more insight into the enhanced performance of the $FAPbI_3$-based PSCs, we compared the properties of the films fabricated by IEP with those obtained from a conventional sequential process. A sequential reaction such as inter-diffusion between FAI/MAI and PbI_2 through thermal annealing in organic iodide/PbI_2 multilayer films has been used to form perovskite $FAPbI_3$/$MAPbI_3$ films from inorganic PbI_2 films in the conventional process (*17*). Thus, considerable volume expansion occurs in the sequential deposition process based on PbI_2 because of the growth of perovskite crystals with the insertion of organic iodides into PbI_2 skeleton (*14*, *22*). As expected, an initial PbI_2 film with thickness of ~ 290 nm was doubled to 570 nm for the film formed by the reaction of PbI_2 with FAI [Table 1 and fig. S6 (*21*)].

In contrast, the change in thickness observed by the application of the FAI (MABr) solution to the pre-deposited PbI_2-(DMSO) film was negligible. In fact, the reaction between FAI (MABr) and PbI_2(DMSO) was completed within 1 min during spin-coating and the $FAPbI_3$ perovskite phase was formed without sequential annealing. However, in a conventional process using PbI_2 films, annealing at high temperature is required to achieve interdiffusion. Figure 3A compares XRD patterns for as-formed and annealed films by IEP and conventional process from PbI_2(DMSO) complex film and PbI_2 film, respectively; there is no appreciable difference in XRD patterns between as-formed and annealed film. This result confirms that the $FAPbI_3$-based layer is formed by the IEP of DMSO and FAI (MABr) without additional annealing process. In addition, such an exchange can considerably favor crystallization into perovskite, compared to conventional interdiffusion from PbI_2, and led to an increase in the XRD peaks intensity after annealing at 150°C for 20 min. However, the as-formed film with PbI_2 showed XRD patterns assigned to PbI_2, FAI, and $FAPbI_3$, and a (002) peak at 12.5° corresponding to the PbI_2 still remains after annealing at same temperature and time with IEP. In particular, the $FAPbI_3$ film prepared by IEP is remarkably preferred (111)-oriented compared to $FAPbI_3$ film annealed after preparing it by conventional process.

The advantages of IEP become further apparent upon comparing the *J-V* curves and PCEs of $FAPbI_3$-based devices derived from PbI_2(DMSO) complex films and conventional PbI_2 films (Fig. 3, B and C). The devices based on $FAPbI_3$ fabricated from PbI_2(DMSO) showed superior PCEs with smaller deviations in the value, compared to those prepared from conventional PbI_2 films. High-efficiency solar cells with average PCEs of over 19% could be produced with a high degree of reproducibility by using the IEP. This study provides an effective protocol for fabricating efficient and cost-effective inorganic-organic hybrid heterojunction solar cells.

REFERENCES AND NOTES

1. J. H. Heo, S. H. Im, J. H. Noh, T. N. Mandal, C.-S. Lim, J. A. Chang, Y. H. Lee, H.-

Kim, A. Sarkar, M. K. Nazeeruddin, M. Grätzel, S. I. Seok, Efficient inorganic-organic hybrid heterojunction solar cells containing perovskite compound and polymeric hole conductors. *Nat. Photonics* **7**, 486–491 (2013). doi:10.1038/nphoton.2013.80

2. H.-S. Kim, C.-R. Lee, J.-H. Im, H.-S. Kim, H.-S. Kim, H.-S. Kim, Lead iodide perovskite sensitized all-solid-state submicron thin film mesoscopic solar cell with efficiency exceeding 9%. *Sci. Rep.* **2**, 591 (2012).

3. M. M. Lee, J. Teuscher, T. Miyasaka, T. N. Murakami, H. J. Snaith, Efficient hybrid solar cells based on meso-superstructured organometal halide perovskites. *Science* **338**, 643–647 (2012). Medline doi:10.1126/science.1228604

4. J. Burschka, N. Pellet, S. J. Moon, R. Humphry-Baker, P. Gao, M. K. Nazeeruddin, M. Grätzel, Sequential deposition as a route to high-performance perovskite-sensitized solar cells. *Nature* **499**, 316–319 (2013). Medline doi:10.1038/nature12340

5. N. J. Jeon, J. H. Noh, Y. C. Kim, W. S. Yang, S. Ryu, S. I. Seok, Solvent engineering for high-performance inorganic-organic hybrid perovskite solar cells. *Nat. Mater.* **13**, 897–903 (2014). Medline doi:10.1038/nmat4014

6. M. Liu, M. B. Johnston, H. J. Snaith, Efficient planar heterojunction perovskite solar cells by vapour deposition. *Nature* **501**, 395–398 (2013). Medline doi:10.1038/nature12509

7. J. H. Noh, S. H. Im, J. H. Heo, T. N. Mandal, S. I. Seok, Chemical management for colorful, efficient, and stable inorganic-organic hybrid nanostructured solar cells. *Nano Lett.* **13**, 1764–1769 (2013). Medline

8. J. W. Lee, D. J. Seol, A. N. Cho, N. G. Park, High-efficiency perovskite solar cells based on the black polymorph of $HC(NH_2)_2PbI_3$. *Adv. Mater.* **26**, 4991–4998 (2014). Medline doi:10.1002/adma.201401137

9. N. Pellet, P. Gao, G. Gregori, T.-Y. Yang, M. K. Nazeeruddin, J. Maier, M. Grätzel, Mixed-organic-cation perovskite photovoltaics for enhanced solar-light harvesting. *Angew. Chem. Int. Ed. Engl.* **53**, 3151–3157 (2014). Medline doi:10.1002/anie.201309361

10. N. J. Jeon, J. H. Noh, W. S. Yang, Y. C. Kim, S. Ryu, J. Seo, S. I. Seok, Compositional engineering of perovskite materials for high-performance solar cells. *Nature* **517**, 476–480 (2015). Medline doi:10.1038/nature14133

11. G. E. Eperon, S. D. Stranks, C. Menelaou, M. B. Johnston, L. M. Herz, H. J. Snaith, Formamidinium lead trihalide: A broadly tunable perovskite for efficient planar heterojunction solar cells. *Energy Environ. Sci.* **7**, 982–988 (2014). 10.1039/C3EE43822H doi:10.1039/c3ee43822h

12. T. M. Koh, K. Fu, Y. Fang, S. Chen, T. C. Sum, N. Mathews, S. G. Mhaisalkar, P. P. Boix, T. Baikie, Formamidinium-containing metal-halide: An alternative material for near-IR absorption perovskite solar cells. *J. Phys. Chem. C* **118**, 16458–16462 (2014). doi:10.1021/jp411112k

13. S. Pang, H. Hu, J. Zhang, S. Lv, Y. Yu, F. Wei, T. Qin, H. Xu, Z. Liu, G. Cui, $NH_2CH{=}NH_2PbI_3$: An alternative organolead iodide perovskite sensitizer for mesoscopic solar cells. *Chem. Mater.* **26**, 1485–1491 (2014). doi:10.1021/cm404006p

14. Q. Chen, H. Zhou, Z. Hong, S. Luo, H. S. Duan, H. H. Wang, Y. Liu, G. Li, Y. Yang, Planar heterojunction perovskite solar cells via vapor-assisted solution process. *J. Am. Chem. Soc.* **136**, 622–625 (2014). Medline doi:10.1021/ja411509g

15. P. W. Liang, C. Y. Liao, C. C. Chueh, F. Zuo, S. T. Williams, X. K. Xin, J. Lin, A. K. Jen, Additive enhanced crystallization of solution-processed perovskite for highly efficient planar-heterojunction solar cells. *Adv. Mater.* **26**, 3748–3754 (2014). Medline doi:10.1002/adma.201400231

16. J. H. Im, I. H. Jang, N. Pellet, M. Grätzel, N. G. Park, Growth of $CH_3NH_3PbI_3$ cuboids with controlled size for high-efficiency perovskite solar cells. *Nat. Nanotechnol.* **9**, 927–932 (2014). Medline doi:10.1038/nnano.2014.181

17. Y. Wu, A. Islam, X. Yang, C. Qin, J. Liu, K. Zhang, W. Peng, L. Han, Retarding the crystallization of PbI_2 for highly reproducible planar-structured perovskite solar cells via sequential deposition. *Energy Environ. Sci.* **7**, 2934–2938 (2014). doi:10.1039/C4EE01624F

18. F. Wang, H. Yu, H. Xu, N. Zhao, $HPbI_3$: A new precursor compound for highly efficient solution-processed perovskite solar cells. *Adv. Funct. Mater.* **25**, 1120–1126 (2015). doi:10.1002/adfm.201404007

19. H. Miyamae, Y. Numahata, M. Nagata, The crystal structure of lead(II) iodide-dimethylsulphoxide(1/2), $PbI_2(dmso)_2$. *Chem. Lett.* **9**, 663–664 (1980). doi:10.1246/cl.1980.663

20. J. Selbin, W. Bull, L. Holmes Jr., Metallic complexes of dimethylsulphoxide. *J. Inorg. Nucl. Chem.* **16**, 219–224 (1961). doi:10.1016/0022-1902(61)80493-4

21. See supplementary materials on *Science* Online.

22. L. Hu, J. Peng, W. Wang, Z. Xia, J. Yuan, J. Lu, X. Huang, W. Ma, H. Song, W. Chen, Y.-B. Cheng, J. Tang, Sequential deposition of $CH_3NH_3PbI_3$ on planar NiO film for efficient planar perovskite solar cells. *ACS Photonics* **1**, 547–553 (2014). doi:10.1021/ph5000067

23. H. J. Snaith, A. Abate, J. M. Ball, G. E. Eperon, T. Leijtens, N. K. Noel, S. D. Stranks, J. T.-W. Wang, K. Wojciechowski, W. Zhang, Anomalous hysteresis in perovskite solar cells. *J. Phys. Chem. Lett.* **5**, 1511–1515 (2014). doi:10.1021/jz500113x

24. J. M. Frost, K. T. Butler, F. Brivio, C. H. Hendon, M. van Schilfgaarde, A. Walsh, Atomistic origins of high-performance in hybrid halide perovskite solar cells. *Nano Lett.* **14**, 2584–2590 (2014). Medline doi:10.1021/nl500390f

ACKNOWLEDGMENTS

This work was supported by the Global Research Laboratory (GRL) Program, the Global Frontier R&D Program on Center for Multiscale Energy System funded by the National Research Foundation in Korea, and by a grant from the KRICT 2020 Program for Future Technology of the Korea Research Institute of Chemical Technology (KRICT), Republic of Korea.

SUPPLEMENTARY MATERIALS

www.sciencemag.org/cgi/content/full/science.aaa9272/DC1
Materials and Methods
Figs. S1 to S6

14 February 2015; accepted 30 April 2015
Published online 21 May 2015
10.1126/science.aaa9272

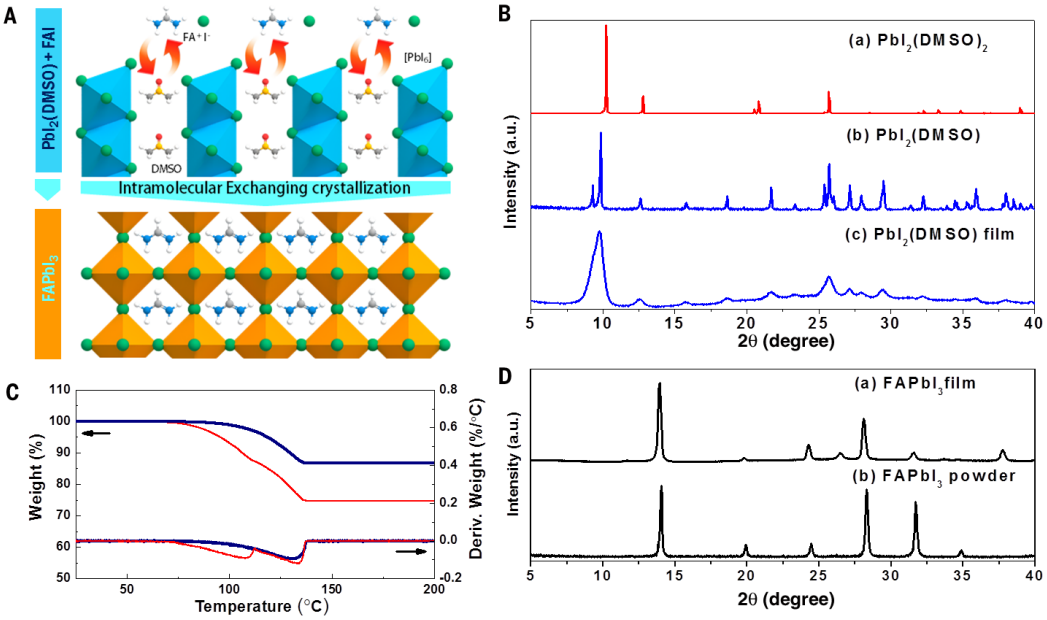

Fig. 1. PbI_2-complex formation and X-ray diffraction. (**A**) Schematics of $FAPbI_3$ perovskite crystallization involving the direct intramolecular exchange of dimethylsulfoxide (DMSO) molecules intercalated in PbI_2 with formamidinium iodide (FAI). The DMSO molecules are intercalated between edge-sharing $[PbI_6]$ octahedral layers. (**B**) XRD patterns of (a) as-prepared $PbI_2(DMSO)_2$ powders, (b) vacuum-annealed $PbI_2(DMSO)$ powders, and (c) as-deposited film on fused quartz substrate using $PbI_2(DMSO)$ complex solution. (**C**) TGA of $PbI_2(DMSO)_2$ (red line) and $PbI_2(DMSO)$ (dark blue line). (**D**) XRD patterns of (a) as-formed film of $FAPbI_3$ by IEP, and (b) $FAPbI_3$ powder.

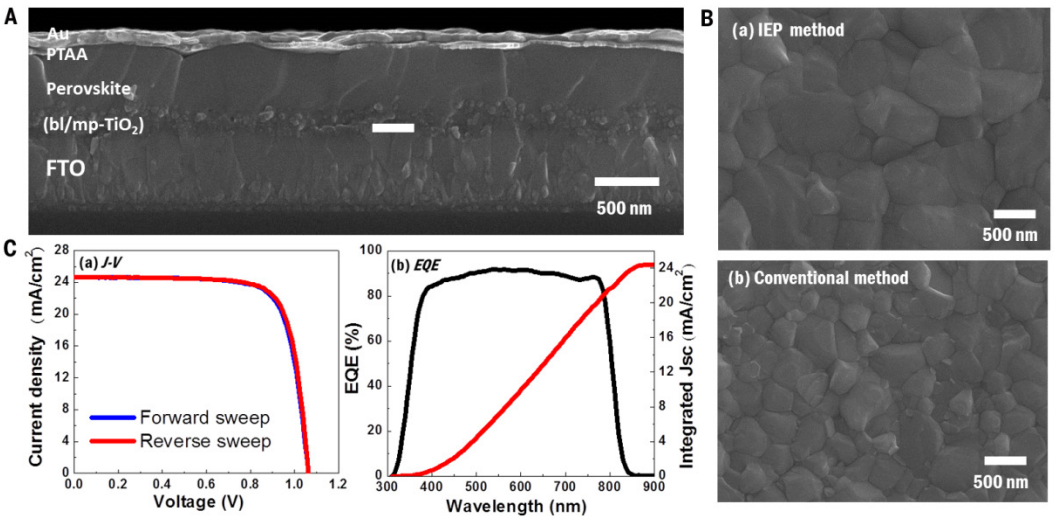

Fig. 2. SEM observation, I-V and EQE measurements. (**A**) Cross-sectional FESEM image of the device consisting of FTO-Glass/bl-TiO_2/mp-TiO_2/perovskite/PTAA/Au. (**B**) The comparison of FESEM surface images of $FAPbI_3$-based layer formed on mp-TiO_2 by IEP and conventional method. (**C**) (a) *J-V* curves of best device measured with a 40 ms scanning delay in reverse (from 1.2 V to 0 V) and forward (from 0 V to 1.2 V) modes under standard AM 1.5G illumination, and (b) EQE spectra for best device and integrated J_{SC}.

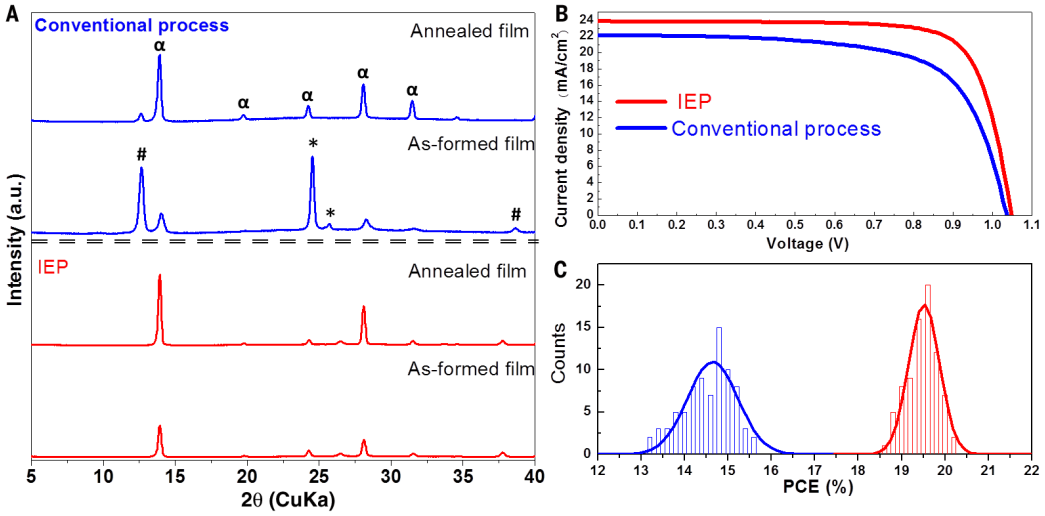

Fig. 3. Comparison of X-ray diffractions, performance, and reproducibility between IEP and conventional process. (**A**) XRD patterns of as-formed and annealed film for $FAPbI_3$-based layers formed by IEP (red line) and conventional (blue line) process. α, #, and * denote the identified diffraction peaks corresponding to the $FAPbI_3$ perovskite phase, PbI_2, and FAI, respectively. (**B**) Representative *J-V* curves for $FAPbI_3$-based cells fabricated by IEP and conventional process. (**C**) Histogram of solar cell efficiencies for each 66 $FAPbI_3$-based cells fabricated by IEP and conventional process.

Table 1. Comparison of layer thickness before and after $FAPbI_3$ phase is formed by conventional and intramolecular exchange process. The thin PbI_2 and PbI_2(DMSO) layers were deposited on a fused quartz glass, and their layer thickness was measured by alpha-step IQ surface profiler.

Method	Before	After
Conventional process (PbI_2)	290 nm	570 nm
IEP (PbI_2(DMSO))	510 nm	560 nm